Structural, morphological and electrical characterization of ceria-based nanostructured thin films obtained by ultrasonic spray pyrolysis

Rubén Martínez-Bautista[a], Suilma M. Fernández-Valverde[b], Adriana Tejeda-Cruz[a], José A. Chávez-Carvayar[a],*

[a] Instituto de Investigaciones en Materiales, UNAM, Ciudad de México, México
[b] Departamento de Química, Instituto Nacional de Investigaciones Nucleares, Ciudad de México, México

ARTICLE INFO

ABSTRACT

In this work, the synthesis and the structural, morphological and electrical characterization of $Ce_{1-x}Sm_xO_{2-\delta}$ solid solution, with $x = 0$, 0.10, 0.15, 0.20, 0.25 and 0.30 mol, are reported. Nanocrystalline, homogeneous, and adherent samarium doped cerium oxide thin films were deposited onto glass (Pyrex®) substrates by a simple and cost effective ultrasonic spray pyrolysis system, at a low substrate temperature of 450 °C and further annealing treatment at 500 °C for 2 h. For all the samples, X-ray diffraction results showed the formation of single phase and well crystalline thin films, with cubic fluorite type structure. Scanning electron microscopy analyses showed homogeneous surfaces for all the samples; from SEM micrographs crystallite sizes were found to be in the range 23–37 nm. From atomic force microscopy, surface roughness in the range of 20–95 nm was measured and the formation of smooth films with an average grain size of 45 nm was observed. For the best sample in the solid solution, high oxygen ion conductivity of 1.71×10^{-1} S cm^{-1}, at 450 °C, was determined by impedance spectroscopy, with an activation energy of 0.93 eV. Results suggest that these films may have a potential application as electrolytes in intermediate temperature solid oxide fuel cells, IT-SOFC.

Caracterización estructural, morfológica y eléctrica de películas delgadas nanoestructuradas a base de ceria, obtenidas por rocío pirolítico ultrasónico

RESUMEN

En este trabajo se reporta la síntesis y caracterización estructural, morfológica y eléctrica de la solución sólida $Ce_{1-x}Sm_xO_{2-\delta}$, con $x = 0$, 0,10, 0,15, 0,20, 0,25 y 0,30 mol. Se depositaron películas delgadas de óxido de cerio dopado con samario nanoestructuradas, homogéneas y con buena adherencia sobre sustratos de vidrio (Pyrex®) mediante un sistema de rocío pirolítico ultrasónico sencillo y económico, a una baja temperatura de 450 °C y con un tratamiento térmico adicional a 500 °C por 2 h. Para todas las muestras, los resultados

* Corresponding author.
E-mail address: josech@unam.mx (J.A. Chávez-Carvayar).

obtenidos por difracción de rayos X mostraron la presencia de películas delgadas cristalinas monofásicas, con estructura cúbica tipo fluorita. Los análisis de microscopía electrónica de barrido mostraron superficies homogéneas para todas las muestras; a partir de las micrografías SEM se determinó que los tamaños de los cristales se encontraban en el intervalo de 23-37 nm. A partir de microscopía de fuerza atómica se midió la rugosidad superficial en el rango de 20 a 95 nm y se observó la formación de películas homogéneas con un tamaño promedio de grano de 45 nm. Para la mejor muestra, mediante espectroscopia de impedancias se determinó una alta conductividad de iones de oxígeno de $1{,}71 \times 10^{-1}\,\mathrm{S\,cm^{-1}}$, a 450 °C, con una energía de activación de 0,93 eV. Los resultados sugieren que estas películas pueden tener una potencial aplicación como electrolitos en celdas de combustible de óxidos sólidos de temperatura intermedia, IT-SOFC.

Introduction

In recent years, solid oxide fuel cells (SOFC) have been of interest to the scientific community due to their ability to promote clean, green and high efficiency energy conversion [1–5]. However, the high operating temperature, around 1000 °C, makes the selection of materials very limited. On the other hand, two of the main research goals for SOFC are the efficiency improvement and the reduction of the operation temperature of these devices, by an appropriate selection of materials [6–8]. Efficiency is mainly related to the improvement of electrolyte materials, which must have high ionic conductivity, high chemical stability, high density and must to be thin materials. Among those materials that can be used as solid electrolytes, because of their important advantages like long-term stability and economical competitiveness [9], ceria-based materials have been widely studied as the alternative for yttrium stabilized zirconia (YSZ) commonly used as electrolyte in SOFC. Furthermore, samarium doped cerium (SDC) thin films may reduce not only the resistance but also the operation temperature of SOFC [10–15].

Several techniques have been used to prepare thin film electrolytes, such as screen printing [16], tape casting [17], pulse laser deposition [18], cathodic sputtering [19], electron deposition (EB-PVD) [12], and spray pyrolysis [20–26]. Among these methods, spray pyrolysis is a simple, low cost and integrated process to produce large area and well adherence films with controlled morphology and uniform thickness.

Spray pyrolysis consists of three consecutive steps, after atomization of a liquid precursor containing metal salts into droplets, they travel toward a heated substrate and film formation occurs and, finally, the evaporation of the solvent and decomposition of the deposited material takes place [27–30].

This technique, under ambient pressure, provides high flexibility in terms of the materials composition, it is an appropriate method for the deposition of a wide variety of thin films since the addition of dopants to the spray solution is simple it is easy to prepare films of any composition by simply mixing the components in the appropriate ratios [20].

In this research, dense and homogeneous nanocrystalline $Ce_{1-x}Sm_xO_{2-\delta}$ thin films, with $x = 0$, 0.10, 0.15, 0.20, 0.25 and 0.30 mol, were successfully deposited by ultrasonic spray pyrolysis technique, at low substrate temperature of 450 °C.

The structural, morphological and transport properties of annealed films, at 500 °C for 2 h, are reported.

Experimental procedure

Thin films preparation

A typical ultrasonic spray pyrolysis (USP) system is shown in Fig. 1. The nebulizer delivers ultrasonic waves generated by the high frequency vibration (1.7 MHz) of a piezoelectric transducer in order to atomize the precursor chemical solution into a stream of fine droplets, 1–5 µm.

Cerium (III) acetylacetonate hydrate $Ce(C_5H_7O_2)_3 \cdot xH_2O$ (Sigma Aldrich, 99.9%) and Samarium (III) acetylacetonate hydrate $C_{15}H_{21}SmO_6 \cdot xH_2O$ (Sigma Aldrich, 99.9%) in appropriate amounts, and dissolved in 0.036 M dimethylformamide HCON $(CH_3)_2$ (J. T. Baker, 99.93%), were used as reactive precursors.

To obtain $Ce_{1-x}Sm_xO_{2-\delta}$ thin films, after precursor chemical solutions were prepared they were carried under an air flow of 120 mL/min and a scanning speed of 0.005 m/s to the substrates, which were kept at 1 cm from the nozzle. Films were deposited onto glass substrates (2 cm × 2 cm) previously ultrasonically cleaned, in ethanol, for 10 min. Deposited films were allowed to cool slowly and then placed in a desiccator.

In the ultrasonic spray pyrolysis method, the substrate temperature plays an important role for phase formation and crystallinity of the films. To obtain the optimal value, substrate temperature was varied in the range 350–450 °C with an interval of 50 °C. In order to study the effect of annealing temperature on phase formation and crystallinity of the products, films, which were deposited under above mentioned substrate temperature, were annealed at 450 °C and 500 °C, for 2 h each.

Structural and morphological characterization

X-ray diffraction (XRD) is a powerful technique not only to identify the crystalline structure of materials but also to analyze several structural properties such as phase composition, grain size, preferred orientation, strain, and defect structure. Thin films were analyzed by XRD technique using a Siemens D500 diffractometer, with $CuK\alpha_1$ radiation, $\lambda = 1.54056$ Å. The operation conditions of the diffractometer were 34 kV and
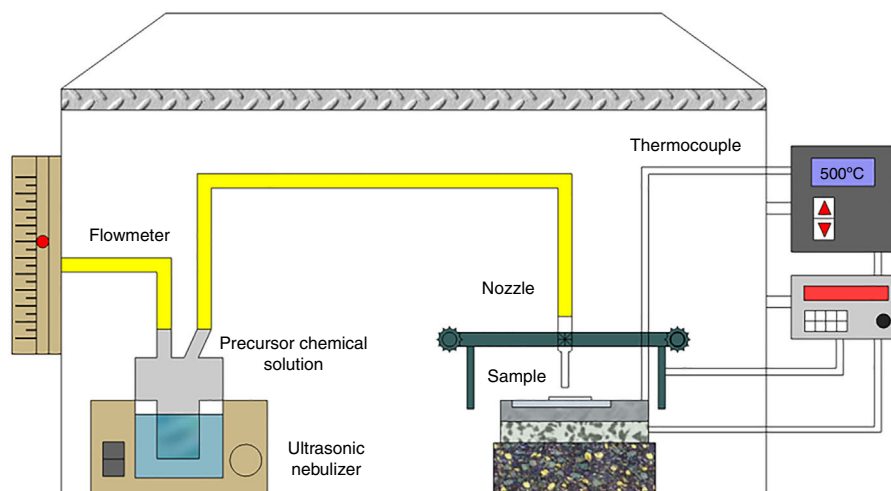
Fig. 1 – Experimental setup used for ultrasonic spray pyrolysis depositions.

25 mA to produce an intense X-ray beam whose incidence angle was 1°. Step size and time/step were 0.02° and 1.2 s, respectively. Measurements were performed from 20 to 70 2θ degrees. Phases in all compounds were identified using EVA software and ICDD data base (JCPDS cards). OriginLab software was employed for measuring the Full Width at Half Maximum (FWHM) of the most intense peaks to calculate the crystallite size (d) by using the Scherrer equation

$$d = \frac{0.9\lambda}{\beta \cos \theta},$$ (1)

where λ is the X-ray wavelength, β is the FWHM of the peaks and θ is the diffraction angle.

Morphological characterization of thin films was performed with a field emission scanning electron microscopy (SEM) JEOL JSM 7600F, equipped with X-ray energy detector X-ACT Oxford INCA for chemical analyses. Working conditions included a low accelerating voltage from 1 to 5 kV, and work distances in the range 4–10 mm. The obtained images were acquired with secondary electrons.

In order to complete the morphological characterization, atomic force microscopy (AFM) technique was carried out. Analyses were performed with a microscope JEOL JSPM-4210. Images were obtained in tapping mode and results were analyzed using the WinSPM DPD software version 2.0.

Transport properties

Transport properties of thin films were performed by impedance spectroscopy technique. Impedance measurements of films were carried out in air between 150 and 500 °C in the frequency range from 0.1 Hz to 10 MHz, using a Solartron 1260 Impedance Analyzer attached with a 1296 Dielectric Interface. Two small parallel areas, which were used as electrodes, were made on the surface of thin films with carbon paste (PELCO high temperature carbon paste, Ted Pella, Inc.). Conductivities of thin films were determined using the Z-View software, from Nyquist plots results were modeled as parallel equivalent circuits connected in series.
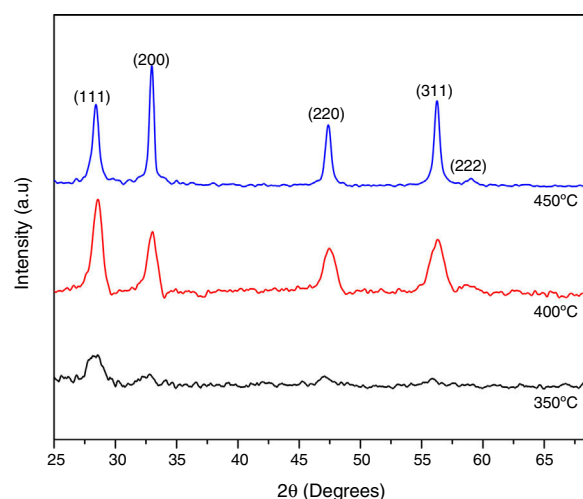

Fig. 2 – XRD patterns of Ce$_{0.80}$Sm$_{0.20}$O$_{2-\delta}$, at different synthesis temperatures, showing the kinetic growth of deposited films.

Results and discussion

Structural analysis

To obtain high quality Ce$_{1-x}$Sm$_x$O$_{2-\delta}$ compounds, the substrate temperature for the deposition of thin films was varied in the range 350–450 °C, with steps of 50 °C, and the kinetic growth was analyzed by XRD to identify the best substrate and annealing temperatures. For 350 °C, compounds showed a partial amorphous nature probably because the decomposition of the precursor solutions have not been completed, however the substrate temperature strongly affects the growth of (111) and (200) peaks, when temperature reaches 400 °C the preferred orientation changes to (200) plane. When the substrate temperature increases, the films become more crystallite, as indicated by the increased intensity of the (200) peak however the corresponding FWHM decreased, Fig. 2. From these
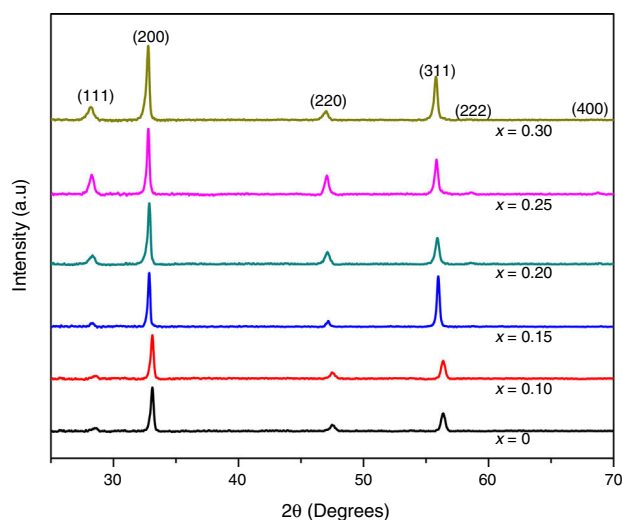
Fig. 3 – XRD patterns of $Ce_{1-x}Sm_xO_{2-\delta}$ thin films synthesized al 450 °C and sintered at 500 °C for 2 h.

Fig. 4 – SEM micrograph of $Ce_{0.8}Sm_{0.2}O_{2-\delta}$ thin film synthesized at 400 °C without heating treatment.

Table 1 – For $Ce_{1-x}Sm_xO_{2-\delta}$ thin films: (a) average grain size, d, calculated from Scherrer's equation. (b) Lattice parameters, a, obtained with CELREF software. (c) Average grain size, d, obtained from SEM images.

x	(a) d (nm)	(b) a (Å)	(c) d (nm)
0	31	5.407 ± 0.004	23
0.10	31	5.422 ± 0.004	35
0.15	41	5.436 ± 0.004	37
0.20	34	5.447 ± 0.004	37
0.25	38	5.459 ± 0.004	32
0.30	31	5.465 ± 0.004	24

results, optimized substrate temperature for the deposition of $Ce_{1-x}Sm_xO_{2-\delta}$ thin films was found to be 450 °C, also the crystallinity was enhanced with a further thermal treatment at 500 °C for 2 h. From now these conditions, 450 °C for synthesis and 500 °C for annealing temperatures will be taken for all $Ce_{1-x}Sm_xO_{2-\delta}$ thin films.

XRD patterns of samarium doped ceria thin films are shown in Fig. 3. It was found that all compositions are well crystallized single phase products with a cubic fluorite type crystal structure, (ICDD file 04-013-4361), which corresponds to a space group Fm-3m (225). For all compositions, wide peaks in the XRD patterns indicate nanocrystalline products. Also, from XRD results it can be observed that under the deposition conditions, all the samples exhibit preferential orientation along the (200) plane [15,31–33].

The average size of crystallites was calculated by using the Scherrer formula, Eq. (1), to the (111), (200), and (220) diffraction peaks. For all compositions, peak shapes were fitted to a pseudo Voigt function profile. For the most intense peaks, (200), average grain sizes are shown in Table 1a.

Indexing of diffraction patterns was performed using DICVOL [34,35] software with WinplotR/Fullprof package, the cell type and the lattice parameters were determined by the
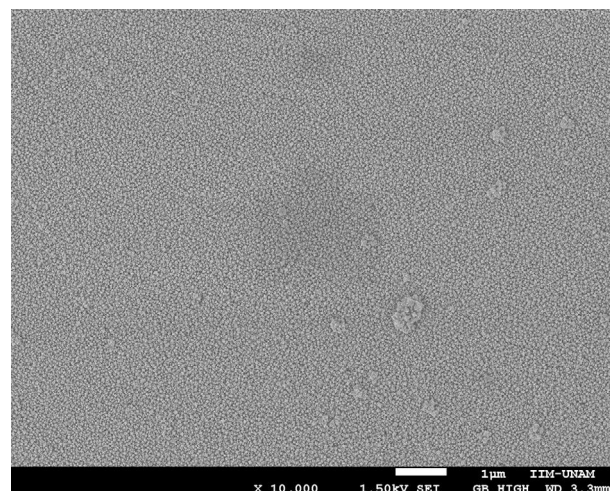
least squares method (CELREF software) [36]. After obtaining the cell parameters a refinement of these values were carried out to minimize the dispersion between experimental and calculated values. Table 1b shows the lattice parameters of $Ce_{1-x}Sm_xO_{2-\delta}$, thin films.

Morphological results

SEM micrograph of $Ce_{0.8}Sm_{0.2}O_{2-\delta}$ thin film, which was synthesized at 400 °C without further heating treatment is shown in Fig. 4. This image shows a surface morphology free of cracks with small agglomerates probably because the decomposition of the precursor solution has not been completed.

SEM micrographs of $Ce_{1-x}Sm_xO_{2-\delta}$ thin films prepared at 450 °C and sintered at 500 °C for 2 h show no cracks, Fig. 5(a)–(d). Uniform surfaces composed of fine grains are clearly observed, which indicate a complete decomposition and evaporation of precursor deposited on the substrates. Screen Caliper software, version 4.0, was used to measure the grain sizes observed in SEM micrographs; results are shown in Table 1c.

High magnification SEM images revealed that $Ce_{1-x}Sm_xO_{2-\delta}$ compounds consist of nanostructured particles around 30 nm in size. This size calculation is rather consistent with the crystallites size determined by XRD using the Scherrer's equation, i.e. the broad peaks appeared in the XRD patterns are due to the presence of nanosized $Ce_{1-x}Sm_xO_{2-\delta}$ crystallites in the films. For all compounds, micrographs show a rough morphology with popcorn shaped clusters, it seems that the addition of samarium promotes a grain growth with triangular shape. At higher magnification, 50 000×, grains of $Ce_{0.85}Sm_{0.15}O_{2-\delta}$ and $Ce_{0.80}Sm_{0.20}O_{2-\delta}$ are slightly larger than those of the other compositions, Fig. 6.

EDX spectra of $Ce_{1-x}Sm_xO_{2-\delta}$ thin films were carried out; for $x > 0$ results confirmed the presence of Ce, Sm and O in all

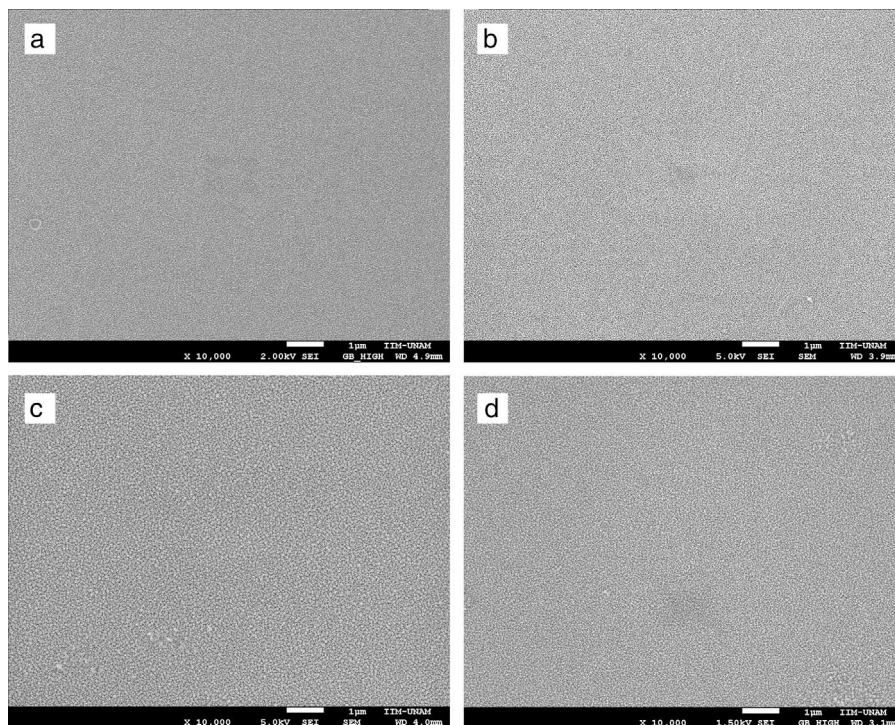**Fig. 5 – SEM micrographs of Ce$_{1-x}$Sm$_x$O$_{2-\delta}$ thin films (synthesized at 450 °C and sintered at 500 °C for 2 h) at 10 000× magnification: (a) x = 0, (b) x = 0.15, (c) x = 0.20, and (d) x = 0.30.**

Fig. 6 – SEM micrographs of Ce$_{1-x}$Sm$_x$O$_{2-\delta}$ thin films (synthesized at 450 °C and sintered at 500 °C for 2 h) at 50 000× magnification: (a) x = 0, (b) x = 0.15, (c) x = 0.20, and (d) x = 0.30.
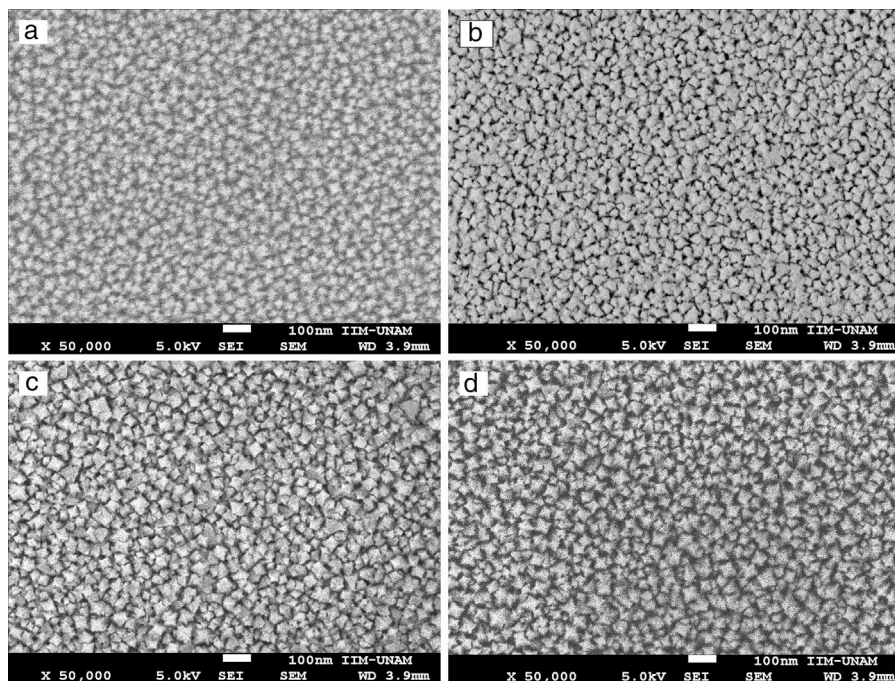
films. The EDX spectrum of Ce$_{1-x}$Sm$_x$O$_{2-\delta}$, for x = 0.2, synthesized at 450 °C and annealed at 500 °C is shown in Fig. 7.

Cross-section micrographs were obtained to determine the thickness of deposited thin films, measured values are in the range 100–350 nm; images also showed dense films

with adequate adhesion to the substrate. The cross-section micrograph of Ce$_{0.80}$Sm$_{0.20}$O$_{2-\delta}$ thin film is shown in Fig. 8.

Additional morphological studies by AFM were carried out. For all samples, the surface roughness and grain sizes of the products were determined. Values for grain sizes were
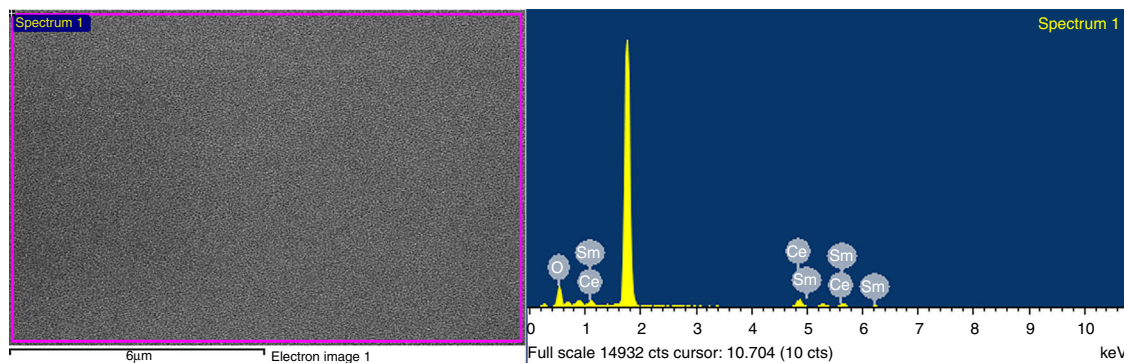
Fig. 7 – Analyzed area, and EDS spectrum of $Ce_{0.80}Sm_{0.20}O_{2-\delta}$ thin film; the most intense peak corresponds to Si (1.739 keV) from the glass substrate.
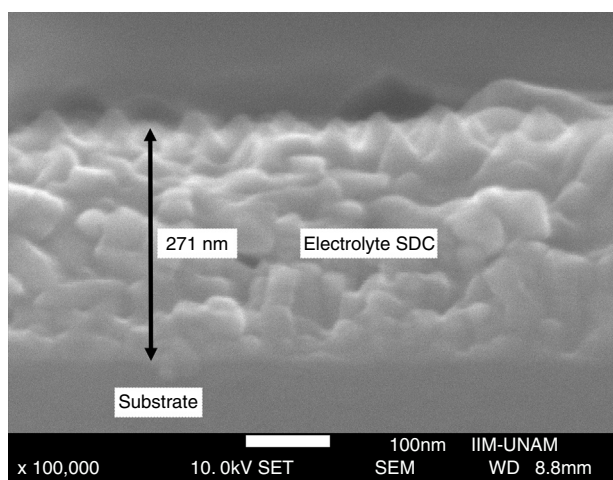

Fig. 8 – SEM micrograph of $Ce_{0.80}Sm_{0.20}O_{2-\delta}$ profile.

obtained using WinSPM DPS software V2.0, and the average roughness of thin films by the formula

$$R_a = \frac{1}{S_0} \int_0^{x_{max}} \int_0^{y_{max}} \left| (f(x,y) - Z_0) \right| dx\, dy, \qquad (2)$$

$f(x, y)$ it is the height of the peaks in the analysis plane, Z_0 is the average height of the peaks in terms of analysis and S_0 is the plane area analysis.

Fig. 9 shows three-dimensional AFM images of the thin films surface topography. In Fig. 9(a) and (c), which belongs to CeO_2 and $Ce_{0.85}Sm_{0.15}O_{2-\delta}$ respectively, high surface homogeneity can be observed. For these films, the surface morphology is composed of small granules with almost spherical shape, which average sizes are 80 and 95 nm. Fig. 9(b) and (d) shows images of $Ce_{0.80}Sm_{0.20}O_{2-\delta}$ and $Ce_{0.70}Sm_{0.30}O_{2-\delta}$, respectively; regular surfaces are also observed but now the average sizes of the agglomerates, 190 and 210 nm, are larger compared to those observed for $x=0$ and $x=0.15$. Average roughness (R_a) was calculated from Eq. (2) for all the films, these values are in the range of 20–95 nm. In this work, the surface morphology shows the formation process of the thin films by using the USP method. After the atomized particles are dispersed toward the surface of the glass, the

temperature of the substrate is such that the finest droplets are likely to react chemically before reaching the substrate and they are grouped one on top of the other until they crystallize, however the homogeneity is adversely affected producing the profile and roughness (R_a) observed on the surface of the films [37], these morphological results are similar to those previously reported by Sriubas and Kwak [12,38].

Two-dimensional AFM images were used to determine the grain sizes of all compounds, measurements indicated that these values are in the range 30–60 nm and agreed those values obtained from SEM micrographs. Fig. 10 shows the AFM profile of $Ce_{0.80}Sm_{0.20}O_{2-\delta}$.

Transport properties

Impedance measurements of thin films were performed in air, in the temperature range 200 °C–500 °C. Typical complex impedance plots (Z' vs $-Z''$), at 400 °C, are shown in Fig. 11. These Nyquist graphs showed only one incomplete arc, which corresponds to grain resistance (R_b). Above 300 °C these arcs are well-resolved, however at higher temperatures bulk resistances gradually decrease and approximately at 500 °C the arcs disappeared. The contribution of the bulk was clearly identified from its high frequency response and characteristic capacitance, calculated of the pF order of magnitude.

Conductivity data were used to calculate the activation energy of thin films with the Arrhenius equation

$$\sigma_T = \sigma_0 \exp\left(\frac{-E_a}{kT}\right) \qquad (3)$$

where E_a is the activation energy for conduction (eV), T is the absolute temperature (Kelvin), k Boltzmann's constant and σ_0 is a pre-exponential factor. In this work, electrode resistances were not considered for the total conductivity calculations. From the $\log \sigma T$ vs 1000/T plots, linear adjustments by least squares were carried out to obtain the activation energies, Fig. 12; these values are in the range reported by Sriubas and Li [13,39] and also even lower than those reported by Virbukas [14].

Although the best conductivity was observed for the sample $Ce_{0.80}Sm_{0.20}O_{2-\delta}$, results showed that the activation energy was minimum for the composition $Ce_{0.85}Sm_{0.15}O_{2-\delta}$. The difference in activation energies of $Ce_{1-x}Sm_xO_{2-\delta}$, in the range
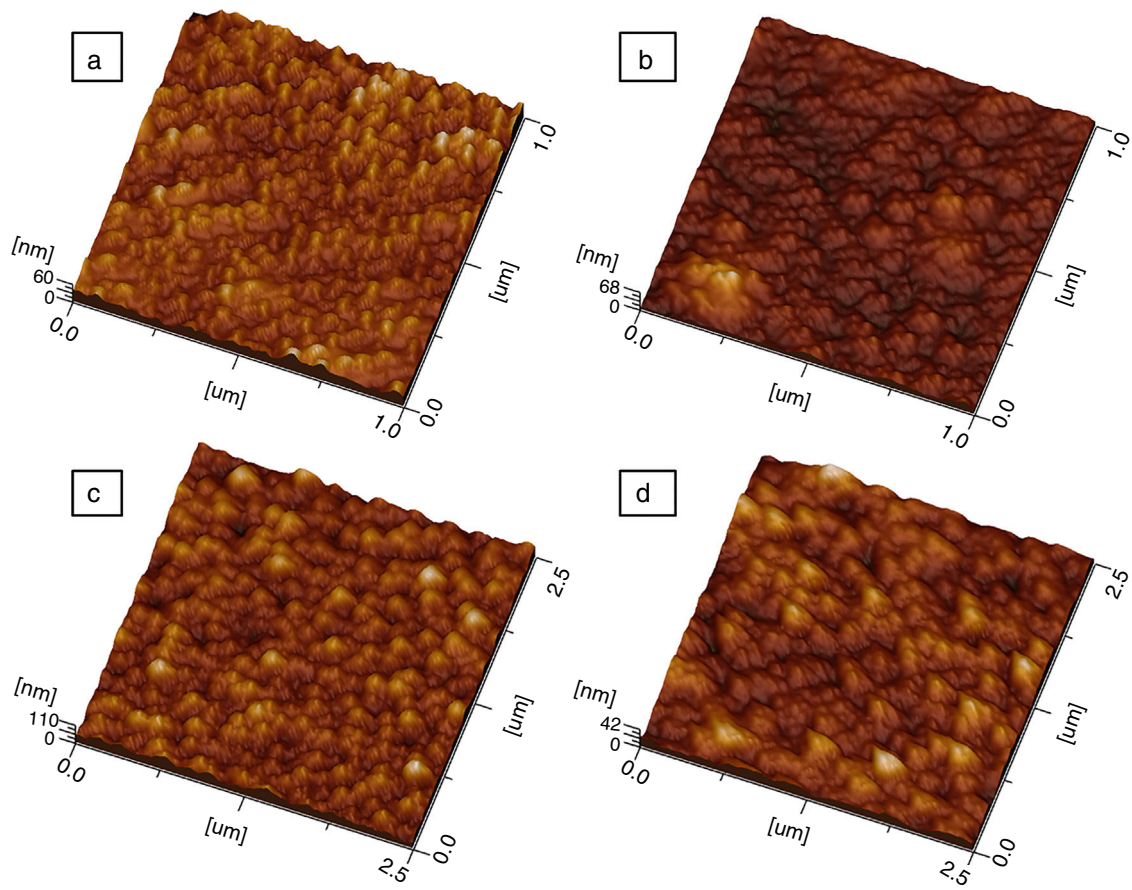
Fig. 9 – 3D AFM micrographs of $Ce_{1-x}Sm_xO_{2-\delta}$ thin films (synthesized at 450 °C and sintered at 500 °C for 2 h): (a) $x = 0$, (b) $x = 0.15$, (c) $x = 0.20$, and (d) $x = 0.30$.
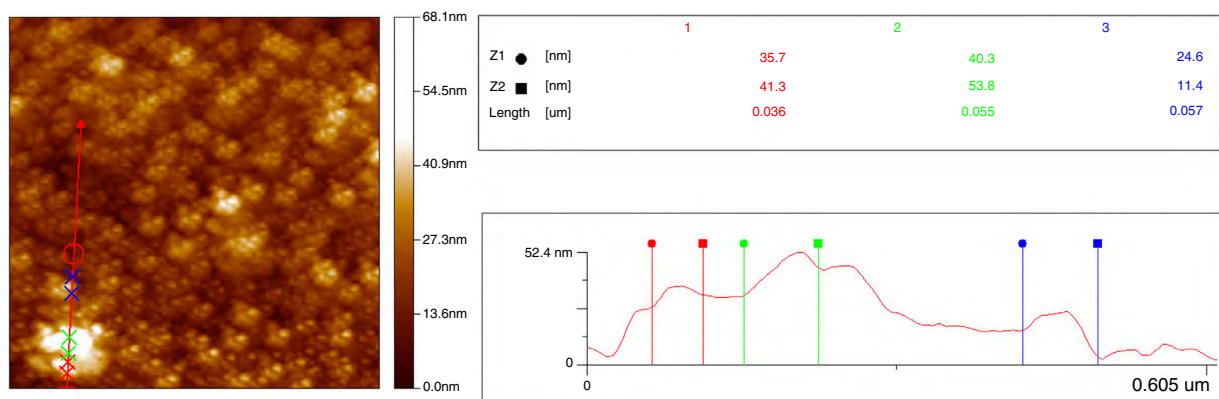

Fig. 10 – AFM profile of $Ce_{0.80}Sm_{0.20}O_{2-\delta}$ thin film, synthesized at 450 °C and sintered at 500 °C for 2 h.

of 0.93 to 1.27 eV, may be attributed to an order-disorder transition of the oxygen sublattice. This decrease is due to the presence of attractive interactions between dopant cations and oxygen vacancies. In fact, it has been mentioned that the activation energy of oxygen vacancy concentration may depend on the dopant since a high concentration of dopants can generate doping grouping and associated oxygen vacancies, which may reduce their mobility. An increase in the RE dopant content for the $Ce_{1-x}Sm_xO_{2-\delta}$ solid solution prevents

oxygen-ordering leading to an increase in activation energy and decrease in ionic conductivity in ceria. Thus, the maximum ionic conductivity and the minimum activation energy are not always associated with the same concentration of dopant [40–43].

Impedance responses were modeled by equivalent circuits using the Zview 3.3 program. The equivalent circuit that fitted the impedance data consisted of a resistor, R_b, and a constant phase element, CPE, connected in parallel. Due to depression
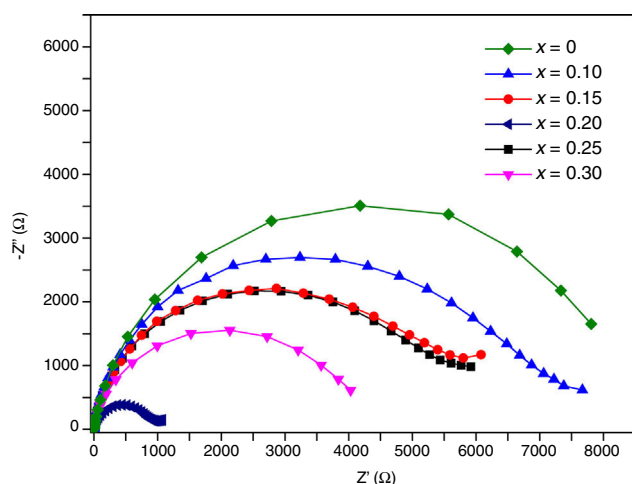
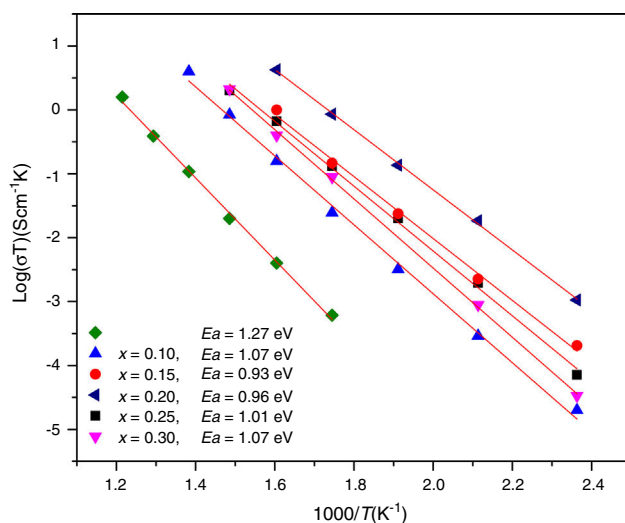**Fig. 11 – Nyquist plots of Ce$_{1-x}$Sm$_x$O$_{2-\delta}$ thin films, synthesized at 450 °C and sintered at 500 °C for 2 h.**

Fig. 12 – Arrhenius plots of total ionic conductivity of Ce$_{1-x}$Sm$_x$O$_{2-\delta}$ thin films, synthesized at 450 °C and sintered at 500 °C for 2 h.

of arcs, the use of a simple capacitor was not sufficient to model the electrical response of thin films, thus a CPE was used to fit these results [44].

Conclusions

The ultrasonic spray pyrolysis technique was satisfactory to deposit nanocrystalline Ce$_{1-x}$Sm$_x$O$_{2-\delta}$ thin films on glass substrates by simple and low cost ultrasonic spray pyrolysis technique. Uniform and dense films were synthesized at temperatures as low as 450 °C, and based on the behavior of the most intense peak, (200), well crystallized compounds were obtained with a further annealing at 500 °C. For all compounds, XRD results showed single phase products with cubic fluorite type structure with space group Fm-3m; it was possible to determine the lattice parameters, and a slight shift to

higher angles was observed with composition, *i.e.* at higher concentration of the dopant the lattice parameter of the compound increased systematically. The average crystalline size calculated by the Scherrer equation was 35 nm. The SEM morphological characterization of thin films depicted uniform homogeneous and crack-free surfaces with pop-corn like structure for all compositions with grain sizes between 23 and 37 nm. For all the films, AFM results showed homogeneous surfaces composed of agglomerates with average sizes in the range 90–210 nm. The transport properties of thin films, which were analyzed by impedance spectroscopy, indicated that the conductivity of these compounds, from 1.71×10^{-1} to 4.43×10^{-4} S cm^{-1} at 450 °C, was dominated by grains, with activation energies in the range 0.93–1.27 eV. Results suggest that these films, in particular those with $x = 0.15$ and 0.20, may be used as solid electrolytes in intermediate temperature solid oxide fuel cells (IT-SOFC).

R E F E R E N C E S

[1] B.B. Patil, S.H. Pawar, Structural, morphological and electrical properties of spray deposited nano-crystalline CeO$_2$ thin films, J. Alloys Compd. 509 (2011) 414–420, http://dx.doi.org/10.1016/j.jallcom.2010.09.045.

[2] K. Amarsingh Bhabu, J. Theerthagiri, J. Madhavan, et al., Cubic fluorite phase of samarium doped cerium oxide (CeO$_2$)$_{0.96}$Sm$_{0.04}$ for solid oxide fuel cell electrolyte, J. Mater. Sci. Mater. Electron. 27 (2016) 1566–1573, http://dx.doi.org/10.1007/s10854-015-3925-z.

[3] J.J. Alvarado Flores, Análisis de la estructura perovskita La$_x$Sr$_{1-x}$Cr$_y$Mn$_{1-y}$O$_{3-\delta}$ con potencial aplicación como ánodo para celdas de combustible de óxido sólido, Boletin de La Sociedad Española de Ceramica y Vidrio 56 (2) (2017) 73–82, http://dx.doi.org/10.1016/j.bsecv.2016.09.003.

[4] S.A. Acharya, V.M. Gaikwad, S.W. D'Souza, S.R. Barman, Gd/Sm dopant-modified oxidation state and defect generation in nano-ceria, Solid State Ionics 260 (2014) 21–29, http://dx.doi.org/10.1016/j.ssi.2014.03.008.

[5] S. Ramesh, G. Upender, K.C.J. Raju, et al., Effect of Ca on the properties of Gd-doped ceria for IT-SOFC, J. Mod. Phys. 4 (2013) 859–863, http://dx.doi.org/10.4236/jmp.2013.46116.

[6] M. Vestli, M. Maide, G. Nurk, E. Lust, Characterization of doped ceria films as SOFC electrolyte prepared by using ultrasonic spray pyrolysis method, ECS Trans. 57 (1) (2013) 1159–1165, http://dx.doi.org/10.1149/05701.1159ecst.

[7] J.A. Gómez-Cuaspud, E. Vera-López, Síntesis and caracterización del sistema La$_{0.8}$Sr$_{0.2}$Ni$_{(1-X)}$Cr$_X$O$_3$ ($x = 0.0, 0.2, 0.4, 0.6, 0.8, 1.0$) por el método de combustión, Boletin de La Sociedad Española de Ceramica y Vidrio 56 (6) (2017) 273–282, http://dx.doi.org/10.1016/j.bsecv.2017.05.004.

[8] G. Nurk, P. Möller, M. Vestli, et al., Mobilty of Sr in gadolinia doped ceria SOFC chemical barrier layers prepared using spray pyrolysis, pulsed laser deposition and magnetron

sputtering methods, ECS Trans. 68 (2015) 1757–1763, http://dx.doi.org/10.1149/06801.1757ecst.

[9] M. Jamshidijam, R.V. Mangalaraja, A. Akbari-Fakhrabadi, et al., Effect of rare earth dopants on structural characteristics of nanoceria synthesized by combustion method, Powder Technol. 253 (2014) 304–310, http://dx.doi.org/10.1016/j.powtec.2013.10.032.

[10] O.S. Khalipova, V. Lair, A. Ringuedé, Electrochemical synthesis and characterization of gadolinia-doped ceria thin films, Electrochim. Acta 116 (2014) 183–187, http://dx.doi.org/10.1016/j.electacta.2013.11.022.

[11] T. Deng, C. Zhang, Y. Xiao, et al., One-step synthesis of samarium-doped ceria and its CO catalysis, Bull. Mater. Sci. 38 (2015) 1149–1154, http://dx.doi.org/10.1007/s12034-015-0994-9.

[12] M. Sriubas, G. Laukaitis, The influence of the technological parameters on the ionic conductivity of samarium doped ceria thin films, Mater. Sci. 21 (2015) 105–110, http://dx.doi.org/10.5755/j01.ms.21.1.5700.

[13] D. Virbukas, M. Sriubas, G. Laukaitis, Structural and electrical study of samarium doped cerium oxide thin films prepared by e-beam evaporation, Solid State Ionics 271 (2015) 98–102, http://dx.doi.org/10.1016/j.ssi.2014.09.036.

[14] D. Virbukas, K. Bočkutė, G. Laukaitis, The electrical and microstructural properties of Zr-doped $LaNbO_4$ thin ceramic films, Mater. Sci. 21 (2015) 439–443, http://dx.doi.org/10.5755/j01.ms.21.3.9535.

[15] T.-S. Oh, S.M. Haile, Electrochemical behavior of thin-film Sm-doped ceria: insights from the point-contact configuration, Phys. Chem. Chem. Phys. 17 (20) (2015) 13501–13511, http://dx.doi.org/10.1039/C4CP05990E.

[16] M.K.M. Ali, K. Ibrahim, E.M. Mkawi, Ag-Al alloy thin film on plastic substrate by screen printing for solar cell back contact application, Mater. Sci. Semicond. Process 16 (2013) 593–597, http://dx.doi.org/10.1016/j.mssp.2012.10.006.

[17] J.-H. Song, S.-I. Park, J.-H. Lee, H.-S. Kim, Fabrication characteristics of an anode-supported thin-film electrolyte fabricated by the tape casting method for IT-SOFC, J. Mater. Process. Technol. 198 (2008) 414–418, http://dx.doi.org/10.1016/j.jmatprotec.2007.07.030.

[18] N. Yang, Y. Shi, S. Schweiger, et al., Role of associated defects in oxygen ion conduction and surface exchange reaction for epitaxial samaria-doped ceria thin films as catalytic coatings, ACS Appl. Mater. Interfaces 8 (2016) 14613–14621, http://dx.doi.org/10.1021/acsami.6b03909.

[19] I. Safi, Recent aspects concerning DC reactive magnetron sputtering of thin films: a review, Surf. Coat. Technol. 127 (2000) 203–218, http://dx.doi.org/10.1016/S0257-8972(00)00566-1.

[20] R. Suresh, V. Ponnuswamy, R. Mariappan, N. Senthil Kumar, Influence of substrate temperature on the properties of CeO_2 thin films by simple nebulizer spray pyrolysis technique, Ceram. Int. 40 (2014) 437–445, http://dx.doi.org/10.1016/j.ceramint.2013.06.020.

[21] M.D. Garza, I. López, I. Gómez, In situ synthesis and deposition of gold nanoparticles with different morphologies on glass and ITO substrate by ultrasonic spray pyrolysis, Adv. Mater. Sci. Eng. (2013) 1–5, http://dx.doi.org/10.1155/2013/916908.

[22] D. Perednis, O. Wilhelm, S.E. Pratsinis, L.J. Gauckler, Morphology and deposition of thin yttria-stabilized zirconia films using spray pyrolysis, Thin Solid Films 474 (2005) 84–95, http://dx.doi.org/10.1016/j.tsf.2004.08.014.

[23] C.Y. Chen, Y.R. Lyu, Effect of NiO addition on properties of bulk yttria-doped ceria sintered from their spray pyrolyzed powder, Ceram. Int. 38 (2012) 3291–3300, http://dx.doi.org/10.1016/j.ceramint.2011.12.036.

[24] S.-J. Shih, Y.-Y. Wu, C.-Y. Chen, C.-Y. Yu, Controlled morphological structure of ceria nanoparticles prepared by spray pyrolysis, Proc. Eng. 36 (2012) 186–194, http://dx.doi.org/10.1016/j.proeng.2012.03.029.

[25] M. De la Garza, I. López, I. Gómez, M.D. Garza, I. López, I. Gómez, In situ synthesis and deposition of gold nanoparticles with different morphologies on glass and ITO substrate by ultrasonic spray pyrolysis, Adv. Mater. Sci. Eng. 2013 (2013) 1–5, http://dx.doi.org/10.1155/2013/916908.

[26] D. Beckel, U.P. Muecke, T. Gyger, et al., Electrochemical performance of LSCF based thin film cathodes prepared by spray pyrolysis, Solid State Ionics 178 (2007) 407–415, http://dx.doi.org/10.1016/j.ssi.2007.01.019.

[27] P.S. Patil, Versatility of chemical spray pyrolysis technique, Mater. Chem. Phys. 59 (1999) 185–198, http://dx.doi.org/10.1016/S0254-0584(99)00049-8.

[28] D. Perednis, L.J. Gauckler, Thin film deposition using spray pyrolysis, J. Electroceram. 14 (2005) 103–111, http://dx.doi.org/10.1007/s10832-005-0870-x.

[29] N. Mahato, A. Banerjee, A. Gupta, S. Omar, K. Balani, Progress in Material Selection for Solid Oxide Fuel Cell Technology: A Review. Progress in Materials Science, Elsevier Ltd., 2015 July 28, http://dx.doi.org/10.1016/j.pmatsci.2015.01.001.

[30] Y. Xie, R. Neagu, C-S. Hsu, et al., Thin film solid oxide fuel cells deposited by spray pyrolysis, J. Fuel Cell Sci. Technol. 7 (2010) 21007, http://dx.doi.org/10.1115/1.3176401.

[31] Y. Jiang, N. Bahlawane, Changes in the structural and optical properties of CeO_2 nanocrystalline films: effect of film thickness, J. Alloys Compd. 485 (2009) 52–55, http://dx.doi.org/10.1016/j.jallcom.2009.06.118.

[32] B. Elidrissi, M. Addou, M. Regragui, et al., Structural and optical properties of CeO_2 thin films prepared by spray pyrolysis, Thin Solid Films 379 (2000) 23–27, http://dx.doi.org/10.1016/S0040-6090(00)01404-8.

[33] J. De Souza, A.G.P. da Silva, H.R. Paes Jr., Synthesis and characterization of CeO_2 thin films deposited by spray pyrolysis, J. Mater. Sci. Mater Electron. 18 (2007) 951–956, http://dx.doi.org/10.1002/crat.201000549.

[34] A. Boultif, D. Louër, Powder pattern indexing with the dichotomy method, J. Appl. Crystallogr. 37 (2004) 724–731, http://dx.doi.org/10.1107/S0021889804014876.

[35] A. Boultif, D. Loueer, Indexing of powder diffraction patterns for low-symmetry lattices by the successive dichotomy method, J. Appl. Crystallogr. 24 (1991) 987–993, http://dx.doi.org/10.1107/S0021889891006441.

[36] A.M.T. Bell, C.M.B. Henderson, R.F. Wendlandt, W.J. Harrison, Rietveld refinement of $Sr_5(AsO_4)_3Cl$ from high-resolution synchrotron data, Acta Crystallogr. Sect. E: Struct. Rep. Online 65 (2009) i16–i17, http://dx.doi.org/10.1107/S1600536809005054.

[37] M. Langlet, J.C. Joubert, The pyrosol process or the pyrolysis of an ultrasonically generated aerosol, in: C.N.R. Raim (Ed.), Chemistry of Advanced Materials, Blackwell, Oxford, 1993, p. 55.

[38] N.W. Kwak, W.C. Jung, Analysis of the grain boundary conductivity of singly and doubly doped CeO_2 thin films at elevated temperature, Acta Mater. 108 (2016) 271–278, http://dx.doi.org/10.1016/j.actamat.2016.02.032.

[39] X. Li, G. Shao, X. Yu, et al., Sintering and electrical properties of $Ce_{0.8}Sm_{0.2}O_{1.9}$ film prepared by spray pyrolysis and tape casting, J. Mater. Sci. Mater. Electron. 22 (2011) 189–192, http://dx.doi.org/10.1007/s10854-010-0112-0.

[40] D.J. Seo, K.O. Ryu, S. Park, Bin, et al., Synthesis and properties of $Ce_{1-x}Gd_xO_{2-x/2}$ solid solution prepared by flame spray pyrolysis, Mater. Res. Bull. 41 (2006) 359–366, http://dx.doi.org/10.1016/j.materresbull.2005.08.012.

[41] B. Steele, Appraisal of $Ce_{1-y}Gd_yO_{2-y/2}$ electrolytes for IT-SOFC operation at 500 °C, Solid State Ionics 129 (2000) 95–110, http://dx.doi.org/10.1016/S0167-2738(99)00319-7.

[42] R. Torrens, N.M. Sammes, G. Tompsett, Characterization of Pr- and Sm-doped $Ce_{0.8}Gd_{0.2}O_{2-\delta}$, J. Electroceram. 13 (2004) 683–689, http://dx.doi.org/10.1007/s10832-004-5176-x.

[43] M.J. VerK, A.J.B.M.J.V Keizer, High oxygen ion conduction in sintered oxides of the Bi_2O_3–Dy_2O_3 system, J. Electrochem. Soc. 128 (1981) 75, http://dx.doi.org/10.1149/1.2127391.

[44] V. Tudić, AC impedance spectroscopy of a-nc-Si:H thin films, Engineering 6 (2014) 449–461, http://dx.doi.org/10.4236/eng.2014.68047.